Clim. Past Discuss., 5, 1901–1928, 2009
www.clim-past-discuss.net/5/1901/2009/


Climate of the Past Discussions

*Climate of the Past Discussions* is the access reviewed discussion forum of *Climate of the Past*

# Pliocene three-dimensional global ocean temperature reconstruction

**H. J. Dowsett, M. M. Robinson, and K. M. Foley**

United States Geological Survey, MS 926A, 12201 Sunrise Valley Drive,
Reston, VA 20192, USA

Received: 8 June 2009 – Accepted: 30 June 2009 – Published: 15 July 2009

Correspondence to: H. J. Dowsett (hdowsett@usgs.gov)

Published by Copernicus Publications on behalf of the European Geosciences Union.





## Abstract

A snapshot of the thermal structure of the mid-Piacenzian ocean is obtained by combining the Pliocene Research, Interpretation and Synoptic Mapping Project (PRISM3) multiproxy sea-surface temperature (SST) reconstruction with bottom water temperature estimates produced using Mg/Ca paleothermometry. This reconstruction assumes a Pliocene water mass framework similar to that which exists today, with several important modifications. The area of formation of present day North Atlantic Deep Water (NADW) was expanded and extended further north toward the Arctic Ocean during the mid-Piacenzian relative to today. This, combined with a deeper Greenland-Scotland Ridge, allowed a greater volume of warmer NADW to enter the Atlantic Ocean. In the Southern Ocean, the Polar Front Zone was expanded relative to present day, but shifted closer to the Antarctic continent. This, combined with at least seasonal reduction in sea ice extent, resulted in decreased Antarctic Bottom Water (AABW) production (relative to present day) as well as possible changes in the depth of intermediate waters. The reconstructed mid-Piacenzian three-dimensional ocean was warmer overall than today, and the hypothesized aerial extent of water masses appears to fit the limited stable isotopic data available for this time period.

## 1 Introduction

Future warming projected by the Intergovernmental Panel on Climate Change (IPCC) (Jansen et al., 2007) poses large socioeconomic impacts to the world community (Robinson et al., 2008a). Thus, the ability to plan for future climate change is a national if not a global priority. Researching, interpreting and modeling past warm climate states refines climate models used to project future climate scenarios and facilitates our ability to confidently model future change. At present, however, most fully coupled ocean-atmosphere paleoclimate modeling experiments utilize a modern ocean temperature dataset for initialization due to the lack of available data on past conditions.



CPD

5, 1901–1928, 2009



A three-dimensional ocean temperature reconstruction of a past warmer-than-present climate state is needed to initialize the models to better approximate a warmer global scenario and to shorten start-up time, thus making model runs more cost effective.

The USGS Pliocene Research, Interpretation and Synoptic Mapping (PRISM) Project develops data sets that describe the major elements of the climate system during the mid-Piacenzian, a time recognized by many as a possible, albeit imperfect, analog to future conditions (Dowsett, 2007; Robinson et al., 2008a,b; Salzmann et al., 2008; Dowsett and Robinson, 2009; Dowsett et al., 2009; Sohl et al., 2009). The mid-Piacenzian is particularly relevant to future climate change since it is the most recent period of Earth history that exhibited global mean annual temperatures equivalent to those projected for the end of this century (Jansen et al., 2007).

The PRISM paleoclimate reconstruction contains all major boundary conditions including reconstructions of land ice distribution, sea ice distribution, vegetation, sea surface temperature (SST), sea level and topography and is the most comprehensive and internally consistent reconstruction of any period of Earth history older than the last interglacial. PRISM data are provided to the paleoclimate modeling community through a series of digital data sets as part of the PRISM Data-Model Cooperative, also known as the Pliocene Model Intercomparison Project (PlioMIP) (see Chandler et al., 2008; Robinson et al., 2008a). These data are being used in a number of climate model experiments to help understand the magnitude and cause of Pliocene climate change relative to the present (see Chandler et al., 2008).

Through the addition of key sites, the PRISM SST reconstruction has been updated and refined to better approximate Pliocene climate, particularly in the equatorial Pacific and the northeastern Atlantic Oceans. Also, using new bottom water temperature data, PRISM has developed a three-dimensional global ocean temperature reconstruction that is consistent with both existing data on Pliocene ocean circulation and also the new PRISM SST reconstruction. Here we present a unique reconstruction of global ocean temperature designed to initiate coupled ocean-atmosphere general circulation models of earth climate and an interpretation of mid-Piacenzian water mass behavior.



CPD
5, 1901–1928, 2009



## 2 Mid-Piacenzian warmth and the PRISM time interval

The middle part of the Piacenzian stage of the Pliocene epoch was a period of relatively warm yet variable climate when continental positions were basically the same as at present and much of the extant Pliocene flora and fauna were shifted to higher latitudes suggestive of a global warming (Dowsett, 2007). Warming during this time period, relative to present conditions, increased with increasing latitude. Estimates of atmospheric $CO_2$ concentrations, however, show values only slightly higher than pre-industrial concentrations (Raymo et al., 1996), suggesting that mid-Piacenzian warmth was not driven soley by increases in greenhouse gases, the proposed culprit for current and future warming (Jansen et al., 2007). Instead mid-Piacenzian warmth may have been a response to enhanced meridional oceanic heat transport (Dowsett et al., 1992; Brierley et al., 2009), a change in sill depth allowing enhanced production of Northern Component Water or NCW (Wright and Miller, 1996; Poore et al., 2006), larger and or more frequent tropical storm events (Emanuel, 2001), or some combination of these mechanisms. Many resources are being focused on understanding the causes of mid-Piacenzian global warmth in an attempt to better understand future climate conditions.

The PRISM interval, calibrated to 3.29 Ma to 2.97 Ma (timescale of Gradstein et al., 2004) (Fig. 1), is defined not only by absolute age but also in terms of position relative to biostratigraphic, magnetostratigraphic and stable isotopic zonations. It is a ~300 Ky interval of time within the middle part of the Piacenzian Age of the Pliocene Epoch. In the literature, this interval is frequently referred to as mid-Piacenzian, PRISM "Time Slab" or PRISM Interval. All refer to the interval between the transition of marine oxygen isotope stages M2/M1 and G19/G18 (Shackleton et al., 1995) in the middle part of the Gauss Normal Polarity Chron (C2An), ranging from within C2An2r (Mammoth reversed polarity) to near the bottom of C2An1 (just above Kaena reversed polarity). This interval correlates in part to planktic foraminiferal zones PL3 (*Globorotalia margaritae-Sphaeroidinellopsis seminulina* Interval Zone), PL4 (*Sphaeroidinellopsis seminulina-Dentoglobigerina altispira* Interval Zone) and PL5 (*Dentoglobigerina*

*altispira-Globorotalia miocenica* Interval Zone) of Berggren et al. (1995). It falls within calcareous nannofossil zone NN16 of Martini (1971) or CN12a of Bukry (1973, 1975) (Dowsett and Robinson, 2006).

The PRISM interval occurs prior to the first strong oxygen-isotope excursions, which represent a change toward modern conditions (Northern Hemisphere ice volume increased, polar fronts were strengthened and glacial -interglacial variation intensified) (Sancetta and Silvestri, 1986; Raymo et al., 1989; Hodell and Ciesielski, 1991; Dowsett et al., 1994). While the PRISM interval is easily distinguished from the intervals immediately surrounding it, there is a high degree of variability within the time slab. The 41 ky period of Earth's obliquity dominates the Pliocene climate record (Tiedemann et al., 1994). Other than glacial stages KM2 (c. 3.12 Ma) and G20 (c. 3.01 Ma), benthic foraminiferal oxygen isotope values were either equal to or isotopically lighter than those of today (Shackleton et al., 1995; Lisiecki and Raymo, 2005) (Fig. 1).

## 3 Sea surface temperature estimates

New multiple proxy SST estimates are now available for the sub-polar North Atlantic and Arctic Oceans (Robinson, 2009) and for the low latitude Pacific Ocean (Dowsett and Robinson, 2009) that greatly enhance and extend the PRISM SST reconstruction into regions previously not represented. The resulting PRISM3 SST Reconstruction now utilizes 86 localities (Fig. 2a, Table 1).

PRISM SST estimates are derived using a warm peak averaging methodology to extract the warm phase of climate from the PRISM interval at each location (see Dowsett and Robinson, 2006; Dowsett, 2007). Warm peak averaging, pioneered by Dowsett and Poore (1990), attempts to determine the average peak warming during the PRISM interval. Only estimates meeting some pre-set quality control criteria are used (Dowsett, 2007). A warm peak is defined as a temperature warmer than the estimates surrounding it in a stratigraphic sequence. Thus, all warm peaks are defined, those not meeting quality control are excluded, and the remainders are averaged.

Mg/Ca and alkenone paleotemperature proxies are utilized as Appendix A where faunal data are already available. In these situations, careful analysis of multiple independent proxies are used to verify each other and gain further insight into the structure of the upper water column (e.g. Robinson et al., 2008b; Dowsett and Robinson, 2009). In areas where faunal proxies are missing or do not work, Mg/Ca and alkenone methods are used alone to estimate SST.

While one SST proxy is not intrinsically better than another, we do not feel multiple proxies should necessarily show concordance. The power of a multiple proxy approach is that no two proxies actually measure the same environmental variable in the same way. The power of the technique lies with this diversity. In practical terms, having faunal based SST estimates for winter and summer bracket a mean annual SST alkenone-based estimate, and a Mg/Ca estimate from a signal carrier that lives at depth being slightly cooler than the alkenone-based estimate calibrated to 10 m, gives a much more complete and robust estimate of paleoenvironmental conditions. Looking for statistical agreement between multiple proxies is an oversimplification of the problem and in many cases invalid.

## 4 Bottom water temperature estimates

Data from 27 DSDP and ODP sites, representing conditions ranging from ~1000 m to ~4500 m water depth, are used in our bottom water temperature analysis (Fig. 2c, Table 2; Cronin et al., 2005; Dwyer, 2009; Dwyer and Chandler, 2009). The Atlantic sector has by far the best three-dimensional coverage. Sites in the Pacific Ocean and Indian Ocean sectors are primarily from the Southern Hemisphere. The deep ocean temperature reconstruction is based upon Mg/Ca paleothermometry utilizing the ostracode genus *Krithe*. The Mg/Ca paleothermometry technique and results are described elsewhere (Cronin et al., 2005; Dwyer and Chandler, 2009). For the remainder of this paper, these Mg/Ca data are collectively referred to as the deep ocean temperature data set.





We used a methodology similar to that used for PRISM SST data to extract the warm phase of bottom water temperature from the deep ocean temperature data set. Deep ocean temperature data at each site were ranked, and the highest 10% were averaged to produce the estimates shown in Fig. 2c and d and Table 2. The limited numbers of samples from some deep ocean temperature sites precluded warm peak averaging. Where time series were of sufficient length, a comparison of estimates generated from both techniques showed the deep ocean temperature estimates to fall, as expected, between those that would be obtained using warm peak averaging and the maximum temperature technique of Dowsett et al. (2005).

## 5 PRISM3D ocean reconstruction

Several assumptions are necessary to define the framework of the PRISM3D reconstruction. First, we assume the same general pattern of thermohaline circulation seen in the modern ocean because we find no evidence in the data that would suggest, for example, deep-water formation in the North Pacific during the PRISM interval. Next, we assume an increased flux of warm surface water to the high latitude North Atlantic and adjacent seas during the PRISM interval, suggested by surface temperature estimates from multiple locations (Dowsett et al., 2009) (Fig. 2b) and robust results of $\delta^{13}C$ analyses from records intersecting the PRISM interval arguing for a high flux of paleo North Atlantic Deep Water (NADW) (Wright and Miller, 1996; Poore et al., 2006).

Finally, we assume that the warm phase of the deep ocean temperature data is most likely coupled with the warm peak averaged PRISM SST reconstruction. PRISM's goal is a synoptic reconstruction of a "super interglacial", not mean conditions. This is a significant assumption since high frequency temperature variability can be observed in many of the deep ocean records (Dwyer and Chandler, 2009) and since the ability to correlate millennial scale features from core to core across the globe does not yet exist at a sufficient number of sites (Dowsett and Robinson, 2006).

These assumptions taken together suggest a conceptual model of increased mid-

Piacenzian meridional overturning circulation (MOC) relative to present day, forcing an adjustment in the extent of NADW, Antarctic Bottom Water (AABW) and Antarctic Intermediate Water (AAIW).

### 5.1 Sea surface temperature reconstruction

Surface temperature estimates presented here comprise the PRISM3 SST data set (Dowsett et al., 1999; Dowsett, 2007; Robinson et al., 2008b; Dowsett and Robinson, 2009; Robinson, 2009), based upon 86 DSDP and ODP sites (Fig. 2, Table 1). Contouring the global SST field from so few irregularly spaced data points is a problematic task. Early attempts at automated contouring of the raw data, using algorithms from Middleton (2000), resulted in unrealistic oceanographic solutions. In order to facilitate model – model comparisons, PRISM elected to have researchers most familiar with the data and its strengths and weaknesses produce subjectively contoured datasets using the methodology outlined below. Much of the design of these datasets (e.g. monthly SST and sea ice) clearly goes beyond the resolution of the raw data, but was required by the modeling community.

At each locality, modern SST was subtracted from the PRISM time-slab value in order to produce a mid-Piacenzian SST anomaly for cold and warm seasons. To create a global dataset, these SST anomalies were plotted as individual points on a $2^{\circ} \times 2^{\circ}$ grid representing the Earth. Modern SST contours served as a rough guide to draw anomaly contours around the control points, because it was assumed that the general pattern of modern oceanic surface current systems was present in the mid-Pliocene. Boundaries between anomaly bands were smoothed to create even temperature gradients. Finally, this smoothed, contoured anomaly field was added to the modern SST of Reynolds and Smith (1995) to create mid-Piacenzian February and August SST maps. SSTs for the remaining 10 months of the year were derived by fitting a sine curve to the February and August SST estimates (Dowsett et al., 1996). The 1 December SST anomaly is shown in Fig. 2b.

### 5.2 3-Dimensional ocean temperature reconstruction

The PRISM3D ocean reconstruction is presented at a 4° latitude by 5° longitude resolution at 33 depth layers corresponding to 0, 10, 20, 30, 50, 75, 100, 125, 150, 200, 250, 300, 400, 500, 600, 700, 800, 900, 1000, 1100, 1200, 1300, 1400, 1500, 1750, 2000, 2500, 3000, 3500, 4000, 4500, 5000 and 5500 m. Specific steps in the reconstruction methodology are listed in Appendix A.

Because the PRISM3D reconstruction is designed to initialize coupled ocean-atmosphere general circulation models, it represents a synoptic reconstruction of a prescribed day, arbitrarily chosen to be 1 December. The Levitus and Boyer (1994) modern ocean temperature dataset was transformed into a 4×5 resolution. The PRISM3 November and December monthly SST reconstructions were averaged to approximate the SST for mid-Piacenzian 1 December. A surface-temperature anomaly was created by subtracting the modern 1 December SST field (Reynolds and Smith, 1995) from the Piacenzian 1 December data (Fig. 2b). The surface temperature anomaly was then added to the 0 m layer of Levitus and Boyer (1994) to create the PRISM3D 0 m reconstruction.

Since no data points fall between 0 m and 1100 m in the deep ocean temperature data set, we chose to use a mathematical function that decreases the weight of the surface anomaly with depth down to 1400 m (see Dowsett et al., 2006). Between 900 m and 1400 m that anomaly was further modified based upon data from Sites 592, 754, 1092 and 1236 that we feel represent an adjustment or vertical expansion of paleo AAIW (Fig. 2d). Therefore, we restrict cooler temperatures in the Southern Hemisphere restricted to this depth interval.

In the Atlantic sector of the Southern Ocean, the data at Sites 1085, 1090, 1092 and 704 may indicate warmer paleo NADW that expands further into the region (Fig. 3a) relative to modern day. At present, Site 704 sits in the core of NADW; during the mid-Piacenzian Site 704 shows a strong warm anomaly (Fig. 2c and d). Slight cooling near the upper boundary of NADW and Circum Polar Deep Water (CPDW) (Site 1092) with





slight warming at the lower boundary (Site 1090) would be expected with an expansion of *paleo* NADW.

The production of warmer *paleo* NADW during the mid-Piacenzian is evident from the anomalies at Sites 552, 610 and 607 (Fig. 2c and d). At all three sites, the expansion or increased production of *paleo* NADW at the expense of AABW is seen as a warm anomaly (Fig. 3a and b). This fits well with the documented warming of the sea surface in the region of NADW production and the proposed expansion of *paleo* NADW production to higher latitudes in the Arctic Ocean. It is plausible that a vertical expansion of *paleo* NADW could cause the slight negative anomaly seen at Site 982, currently bathed by Upper NADW.

In the equatorial Atlantic today, Sites 925, 926, 928 and 929 monitor NADW and, at the deepest point (Site 929, 4356 m), the boundary between NADW and AABW. Warm anomalies for the mid-Piacenzian at all sites are in keeping with the hypothesized warmer and stronger flux of *paleo* NADW and diminished (colder) *paleo* AABW production relative to today (Figs. 2c and d and 3b).

Sites 658, 659 and 661 all monitor NADW today, and the warm anomalies at 658 and 661 record the regional mid-Piacenzian warmth shown at most other locations. The slight negative anomaly at Site 659 (~3000 m water depth) does not fit our conceptual model. Because the deep ocean temperature data contain only seven samples from this site (Dwyer, 2009) we do not place high confidence in these temperature estimates.

In the western Pacific, Sites 804, 805, 806 and 1123 monitor Pacific Deep Water (PDW) today, and all show small positive anomalies for the mid-Piacenzian. We interpret these data to indicate the overall warmer conditions of the water masses that mixed to form *paleo* PDW (Fig. 3d).

In the eastern Pacific, Sites 1236, 1239, 1241 and 1237 form a depth transect from the present day boundary of AAIW and Pacific Central Water (PCW) (1236), through PCW (1239 and 1241) to the boundary between PCW and CPDW (1237) (Figs. 2c and d and 3c). In keeping with our hypothetical distribution of mid-Piacenzian water masses, a vertical displacement of AAIW could explain the minor cooling at the top of

this transect while overall warming of PCW is in keeping with the positive anomalies at the three lower sites along the depth transect.

## 6 Discussion

Temperature is not a tracer for water mass. Our reconstruction assumes a modern water mass framework and imposes changes to those water masses based upon the deep ocean temperature data, published literature and our knowledge of mid-Piacenzian sea-surface circulation and temperature. We make reference to modern water masses but are actually referring to the temperature signals of their paleo analogs.

### 6.1 Enhanced mid-Piacenzian NADW

The PRISM3D ocean reconstruction is characterized by enhanced paleo NADW extending further south than modern NADW. Several lines of evidence support this finding. The PRISM3 surface temperature anomaly (Fig. 2) highlights a large area of the subpolar North Atlantic that is warmer than modern. Preliminary climate modeling studies suggest this same region experienced a decrease in precipitation minus evaporation (P-E) which might suggest production of NADW slightly warmer yet more dense due to increased evaporation in the region (Dowsett et al., 2009). Oxygen and carbon isotope data as well as carbonate preservation evidence exists to suggest that prior to 3.0 Ma the production of northern component deep water was higher than after 3.0 Ma or present day (Sarnthein and Fenner, 1988; Raymo et al., 1996; Wright and Miller, 1996; Poore et al., 2006).

Oppo and Fairbanks (1987) generated a mixing equation to estimate the % overflow of NCW, the precursor to modern NADW, through time using the North Atlantic, Southern Ocean and North Pacific as end members

$$\mathrm{NCW} = \frac{\delta^{13}\mathrm{C_{SO}} - \delta^{13}\mathrm{C_{PO}}}{\delta^{13}\mathrm{C_{NA}} - \delta^{13}\mathrm{C_{PO}}} \times 100 \quad (1)$$

where $\delta^{13}C_{SO}$, $\delta^{13}C_{PO}$ and $\delta^{13}C_{NA}$ are $\delta^{13}C$ estimates for the Southern Ocean, Pacific Ocean and North Atlantic, respectively. $\delta^{13}C$ in this instance is used as a measure of nutrient content of deep water; North Atlantic surface water is depleted in nutrients and deep water gains nutrient content with age. While the interpretation of $\delta^{13}C$ is more complicated, Wright and Miller (1996) and more recently (Poore et al., 2006) used $\delta^{13}C$ to calculate an estimate of NCW (using Eq. 1). The results of both studies are relevant to our analysis of mid-Piacenzian deep ocean circulation. Long-term trends in %NCW appear to be related to vertical movements of the Greenland-Scotland Ridge with high NCW production during the PRISM interval followed by a sharp decrease roughly corresponding to the initiation of Northern Hemisphere glaciation (Wright and Miller, 1996; Poore et al., 2006).

In a similar study, Raymo et al. (1996) used carbon and oxygen isotopes to suggest enhanced production of NCW and greater warmth during the mid-Piacenzian. While there are other factors that can affect the interpretation of $\delta^{13}C$ records, these data appear to corroborate an increased warm NCW at the same time as warmer surface ocean conditions.

### 6.2 Restriction and displacement of Antarctic Waters

The Antarctic Front Zone was expanded but positioned further south during the PRISM interval (Barron, 1996a,b). Our reconstruction supports a reduction of AABW production, and restriction to regions south of the equator. Enhanced NADW appears to have been accomplished in the vertical direction as well, and *paleo* AAIW which lies above NADW, was displaced slightly relative to its present day position, which may account for the small negative anomaly seen in the 1000–1300 m depth interval globally (see Fig. 2d).





### 6.3 Mid-Piacenzian thermocline and upwelling behavior

The reconstruction of the upper ocean is based upon the downward propagation of the surface temperature anomaly. While we currently lack direct measurement of the depth of thermocline in the tropical Pacific, the PRISM3 surface reconstruction does include a reduced E-W temperature gradient due to warmer than present day conditions in the eastern equatorial Pacific (Dowsett and Robinson, 2009). The downward propagation of this surface temperature anomaly by our methodology creates a first approximation of a deepening of the thermocline which is documented by Ravelo et al. (2006).

In other mid-latitude upwelling regions of the Pacific Ocean, data exist suggesting warmer nutrient-rich upwelled-water (Dekens et al., 2007). While these data have not yet been incorporated in the PRISM3 SST reconstruction, they may suggest a warmer southern source subsurface water mass.

What does a warmer global ocean mean for climate? Most data on conditions during the Last Glacial Maximum (LGM) suggest a more vigorous ocean circulation than that of today (Marotzke, 2000). Surface ocean warming results in lower surface density in the North Atlantic and therefore a slowdown in the thermohaline circulation (THC). Coupled ocean-atmosphere numerical modeling studies incorporating mid-Piacenzian surface conditions seemingly confirm this mechanism (Haywood and Valdes, 2004). However, coupled model experiments initiated with the Atlantic sector of the PRISM3D deep ocean temperature reconstruction showed that this addition created an increase in MOC. This might be explained by increased surface evaporation in the region of present day NADW formation (Dowsett et al., 2009). A response to the poleward shift and intensification of winds in a warming climate has also been suggested (Toggweiler and Russell, 2008).

The documentation, however sparse, of both surface and deep ocean warming during the mid-Piacenzian is intriguing, especially in light of estimates of continued global warming through the end of this century (Jansen et al., 2007). Numerical models of Earth Climate System remain the best tool for understanding the role of a warmer





ocean circulation system and for understanding the conditions that may result from such a phenomena.

### 6.4 Possible causes of mid-Piacenzian warmth supported by PRISM3D

For two decades the question of the cause of Pliocene warming has eluded investigators. The two most prominent explanations, increased atmospheric concentrations of $CO_2$ and increased meridional ocean heat flux, are attractive. Both mechanisms have different signatures in the sedimentary record, and neither have been clearly detected. It is safe to say that both have had a prominent role on the magnitude of Pliocene warmth, but there are other mechanisms that should be tested using numerical models.

Tectonically forced changes in various ocean gateways played an important role in metering the circulation of water into different ocean basins. The work on the Greenland-Scotland Ridge in the North Atlantic appears to have a significant effect on Neogene deep water production (Wright and Miller, 1996; Poore et al., 2006). Likewise, the depth of the Indonesian throughflow is an important aspect of the paleoceanographic circulation in the Pacific (Cane and Molnar, 2001; Karas et al., 2009). It has long been held that the depth of the Central American Seaway (CAS) has had a profound effect on Northern Hemisphere climate. While the impact of these gateways has been debated and assessed using numerical modeling, a careful evaluation of global bathymetry for the mid-Piacenzian would be a great benefit to future experiments in that it would allow for all gateways to interact as they did in the past, at the time we observe surface and deep ocean warming.

Finally, the role of tropical storms in moving heat from equator to poles may be underestimated in all but the most sensitive Earth System Models and may not have been adequately explored for mid-Piacenzian paleoclimate scenarios (Emanuel, 2001; Sriver and Huber, 2007).

Thus, the ocean temperature reconstruction presented here is a major step forward for coupled model experiments yet at the same time it begs questions about the very

nature and sensitivity of the climate system. New and innovative data sets representing past conditions (e.g. bathymetry) and processes (e.g. tropical storms) may hold the key to understanding the last great episode of global warmth and may therefore help navigate future climate conditions.

## 7 Conclusions

Earth surface conditions during the mid-Piacenzian have been known for some time to be warmer than present day in the mid- and high latitudes. The resolution with which we can reconstruct those surface conditions is increasing as the tools and proxies of paleoclimatology evolve. The deep ocean is not as well known, yet is a fundamental component of the climate system and has become critical to our understanding of this last period of global warming similar in magnitude to what is expected for the end of this century.

Past deep ocean work concentrated on stable isotope analyses of deep-sea sequences through the mid-Piacenzian. These studies show an enhancement of Northern Component Water (NCW) relative to present day from sites in the North Atlantic, Southern Ocean and Pacific. We have utilized direct temperature estimates (Mg/Ca paleothermometry utilizing *Krithe*) from mid-Piacenzian sequences that corroborate the concept of increased production of warmer NCW during this time interval. These temperature data fit well with mid-Piacenzian surface temperatures estimates.

In our opinion, all data point to the generation of warmer NADW, which expanded as a water mass and extended further south toward Antarctica. The polar front zone was expanded yet positioned closer to Antarctica at this time, and AAIW was formed although it was slightly warmer than at present. We speculate that AAIW and AABW did not extend as far north as they do today. This hypothetical model and these temperature data have been used to generate a three dimensional thermal reconstruction of the mid-Piacenzian global ocean which in turn can be used to initiate coupled ocean-atmosphere model experiments or be used in data-model vali-



CPD
5, 1901–1928, 2009



dation work. (Please see the PRISM web site for more information and links to data: http://geology.er.usgs.gov/eespteam/prism/index.html.) Future work must include analysis of the upper waters (depths <1000m) including salinity estimates so that true water mass properties can be documented.

## Appendix A

### PRISM3D Ocean Reconstruction Methodology

PRISM3D SST=Levitus 94 0 m+PRISM3 Dec 1 Anomaly

*Fractions of the surface anomaly were applied at depth to the top 1400 m.*

PRISM3D 10 m=Levitus 94 10 m+PRISM3 1 Dec anomaly (0.985612922)
PRISM3D 20 m=Levitus 94 20 m+PRISM3 1 Dec anomaly (0.925614579)
PRISM3D 30 m=Levitus 94 30 m+PRISM3 1 Dec anomaly (0.883391208)
PRISM3D 50 m=Levitus 94 50 m+PRISM3 1 Dec anomaly (0.821220811)
PRISM3D 75 m=Levitus 94 75 m+PRISM3 1 Dec anomaly (0.763600719)
PRISM3D 100 m=Levitus 94 100 m+PRISM3 1 Dec anomaly (0.717635117)
PRISM3D 125 m=Levitus 94 125 m+PRISM3 1 Dec anomaly (0.678759932)
PRISM3D 150 m=Levitus 94 150 m+PRISM3 1 Dec anomaly (0.644737485)
PRISM3D 200 m=Levitus 94 200 m+PRISM3 1 Dec anomaly (0.586584444)
PRISM3D 250 m=Levitus 94 250 m+PRISM3 1 Dec anomaly (0.537401792)
PRISM3D 300 m=Levitus 94 300 m+PRISM3 1 Dec anomaly (0.494358545)
PRISM3D 400 m=Levitus 94 400 m+PRISM3 1 Dec anomaly (0.420786655)
PRISM3D 500 m=Levitus 94 500 m+PRISM3 1 Dec anomaly (0.358563587)
PRISM3D 600 m=Levitus 94 600 m+PRISM3 1 Dec anomaly (0.304107742)
PRISM3D 700 m=Levitus 94 700 m+PRISM3 1 Dec anomaly (0.255363558)
PRISM3D 800 m=Levitus 94 800 m+PRISM3 1 Dec anomaly (0.211028811)

*AAIW was elevated in the Southern Hemisphere bringing cooler temperatures to shallower depths.*

PRISM3D 900 m=Levitus 94 900 m+PRISM3 1 Dec anomaly (0.170220209) in the Northern Hemisphere; PRISM3D 900 m=Levitus 94 900 m−0.3°C in the Southern Hemisphere.

*Levitus 94 data for 0 m through 900 m is an average of November and December monthly data to represent 1 December conditions; Levitus 94 data for 1000 m through 5500 m is annual average data because monthly data are not provided at these depths by Levitus 94. Presumably, temperatures at these depths don't change monthly.*

PRISM3D 1000 m=Levitus 94 1000 m+PRISM3 1 Dec anomaly (0.132307757) in the Northern Hemisphere; PRISM3D 1000 m=Levitus 94 1000 m−0.3°C in the Southern Hemisphere.

PRISM3D 1100 m=Levitus 94 1100 m+PRISM3 1 Dec anomaly (0.096824449) in the Northern Hemisphere; PRISM3D 1100 m=Levitus 94 1100 m−0.3°C in the Southern Hemisphere Pacific and Indian Oceans, −0.0°C in Atlantic.

PRISM3D 1200 m=Levitus 94 1200 m+PRISM3 1 Dec anomaly (0.063413348) in the Northern Hemisphere; PRISM3D 1200 m=Levitus 94 1200 m−0.3°C in the Southern Hemisphere Pacific and Indian Oceans, −0.0°C in Atlantic.

PRISM3D 1300 m=Levitus 94 1300 m+PRISM3 1 Dec anomaly (0.031794771) in the Northern Hemisphere; PRISM3D 1300 m=Levitus 94 1300 m in the Southern Hemisphere (no change from modern).

*Increased production and temperature of NADW; increased temperatures, especially*





*in the North Atlantic.*

PRISM3D 1400 m=Levitus 94 1400 m+PRISM3 1 Dec anomaly (0.001745004) in the Northern Hemisphere; PRISM3D 1400 m=Levitus 94 1400 m+0.2°C in the Southern Hemisphere.

PRISM3D 1500 m=Levitus 94 1500 m+0.3°C (Mediterranean Sea remains modern)

PRISM3D 1750 m=Levitus 94 1750 m+0.3°C in Atlantic and Pacific Oceans, +0.7°C in Indian (Mediterranean Sea remains modern)

PRISM3D 2000 m=Levitus 94 2000 m+.5°C in Pacific, +1.0°C in Indian and Atlantic Oceans (Mediterranean Sea remains modern)

PRISM3D 2500 m=Levitus 94 2500 m+0.5°C in Pacific, +1.0°C in Indian and Atlantic Oceans (Mediterranean Sea remains modern)

PRISM3D 3000 m=Levitus 94 3000 m+0.3°C everywhere except +1.3°C in equatorial Atlantic and +2.0°C in North Atlantic

PRISM3D 3500 m=Levitus 94 3500 m+0.3°C everywhere except +1.3°C in equatorial Atlantic and +2.0°C in North Atlantic

PRISM3D 4000 m=Levitus 94 4000 m+0.3°C everywhere except +1.3°C in equatorial Atlantic and +2.0°C in North Atlantic

PRISM3D 4500 m=Levitus 94 4500 m+0.3°C everywhere except +1.3°C in equatorial Atlantic and +2.0°C in North Atlantic



CPD
5, 1901–1928, 2009



PRISM3D 5000 m=Levitus 94 5000 m+0.3°C everywhere except +1.3°C in equatorial Atlantic and +2.0°C in North Atlantic

PRISM3D 5500 m=Levitus 94 5500 m+0.3°C everywhere except +1.3°C in equatorial Atlantic and +2.0°C in North Atlantic

*Acknowledgements.* This reconstruction would not have been possible without many conversations and discussions with T. Cronin, G. Dwyer, M. Chandler and A. Haywood. Special thanks to Danielle Stoll for help with figures and illustrations. Rocio Caballero and Karine Renaud helped with various aspects of data reduction. Mg/Ca analyses were performed at Duke University; Alkenone analyses were performed at Brown University. This work was supported by the US Geological Survey Office of Global Change and is a product of the PRISM Project.

## References

Barron, J. A.: Diatom constraints on the position of the Antarctic Polar Front in the middle part of the Pliocene, Mar. Micropaleontol., 27, 195–213, 1996a.

Barron, J. A.: Diatom constraints on sea surface temperatures and sea ice distribution during the middle part of the Pliocene, US Geol. Surv., Open File Rep. 96–713, 45 pp., 1996b.

Berggren, W. A.: The Pliocene time scale: calibration of planktonic foraminiferal and calcareous nannoplankton zones, Nature, 243, 391–397, 1973.

Berggren, W. A.: Late Neogene planktonic foraminiferal biostratigraphy of the Rio Grande Rise (South Atlantic), Mar. Micropaleontol., 2, 265–313, 1977.

Berggren, W. A., Kent, D. V., Swisher, C. C., and Aubry, M. P.: A revised Cenozoic geochronology and chronostratigraphy, in: Geochronology, time scales and global stratigraphic correlation, edited by: Berggren, W. A., Kent, D. V., Aubry, M. P., and Hardenbol, J., Tulsa, Society for Sedimentary Geology Special Publication, 129–212, 1995.

Bukry, D.: Low-latitude coccolith biostratigraphic zonation, Initial Rep. Deep Sea, 15, 685–703, 1973.

Bukry, D.: Coccolith and silicoflagellate Stratigraphy, Northwestern Pacific Ocean, Deep Sea Drilling Project Leg 32, Initial Rep. Deep Sea, 32, 677–701, 1975.





Brierley, C. M., Fedorov, A. V., Zhonghui L., Herbert, T. D., Lawrence, K. T., and LaRiviere, J. P.: Greatly expanded tropical warm pool and weakened Hadley Circulation in the early Pliocene, Science Express, 323(5922), 1714–1718, doi:10.1126/science.1167625, 2009.

Cane, M. and Molnar, P.: Closing of the Indonesian seaway as a precursor to east African aridification around 3–4 million years ago, Nature, 411, 157–162, 2001.

Chandler, M., Dowsett, H., and Haywood, A.: The PRISM model-data cooperative: mid-Pliocene data-model comparisons, PAGES News, 16, 24–25, 2008.

Cronin, T. M., Dowsett, H. J., Dwyer, G. S., Baker P. A., and Chandler, M.: Mid Pliocene deep-sea bottom water temperatures based on ostracode Mg/Ca ratios, Mar. Micropaleontol., 54, 249–261, 2005.

Dekens, P. S., Ravelo, A. C., and McCarthy, M. D.: Warm upwelling regions in the Pliocene warm period, Paleoceanography, 22, PA3211, doi:10.1029/2006PA001394, 2007.

Dowsett, H. J.: The PRISM palaeoclimate reconstruction and Pliocene sea-surface temperature, in: Deep-time perspectives on climate change: marrying the signal from computer models and biological proxies, edited by: Williams, M., Haywood, A. M., Gregory, J., and Schmidt, D., The Micropalaeontological Society Special Publications, The Geological Society of London, 459–480, 2007.

Dowsett, H., Barron, J., and Poore, R.: Middle Pliocene sea surface temperatures: a global reconstruction, Mar. Micropaleontol., 27, 13–25, 1996.

Dowsett, H. J., Barron, J. A., Poore, R. Z., Thompson, R. S., Cronin, T. M., Ishman, S. E., and Willard, D. A.: Middle Pliocene paleoenvironmental reconstruction: PRISM2, US Geol. Surv., Open File Rep., 99–535, 1999.

Dowsett, H. J., Chandler, M. A., Cronin, T. M., and Dwyer, G. S.: Middle Pliocene sea surface temperature variability, Paleoceanography, 20, PA2014, doi:10.1029/2005PA001133, 2005.

Dowsett, H. J., Chandler, M. A., and Robinson, M. M.: Surface temperatures of the mid-Pliocene North Atlantic Ocean: implications for future climate, Philos. T. R. Soc. A, 367, 69–84, 2009.

Dowsett, H. J., Cronin, T. M., Poore, R. Z., Thompson, R. S., Whatley, R. C., and Wood, A. M.: Micropaleontological evidence for increased meridional heat transport in the North Atlantic Ocean during the Pliocene, Science, 258, 1133–1135, 1992.

Dowsett, H. J. and Poore, R. Z.: A new planktic foraminifer transfer function for estimating Pliocene-Holocene paleoceanographic conditions in the North Atlantic, Mar. Micropaleontol., 16, 1–23, 1990.





Dowsett, H. J. and Robinson, M. M.: Stratigraphic framework for Pliocene palaeoclimate reconstruction: the correlation conundrum, Stratigraphy, 3, 53–64, 2006.
Dowsett, H. J. and Robinson, M. M.: Mid-Pliocene equatorial Pacific sea surface temperature reconstruction: a multi-proxy perspective, Philos. T. R. Soc. A, 367, 109–126, 2009.
Dowsett, H. J., Robinson, M. M., Dwyer, G. S., Chandler, M. A., and Cronin, T. M.: PRISM3 DOT1 Atlantic basin reconstruction, US Geol. Surv., Data Series, 189, online available: http://pubs.usgs.gov/ds/2006/189/index.html, 2006.
Dowsett, H., Thompson, R., Barron, J., Cronin, T., Fleming, F., Ishman, S., Poore, R., Willard, D., and Holtz, T.: Joint investigations of the Middle Pliocene climate I: PRISM paleoenvironmental reconstructions, Global Planet. Change, 9, 169–195, 1994.
Dwyer, G. S.: DSDP 592 and ODP 754, 804, 805, 806, 928, 929, 982, 1085, 1090, 1092, 1123, 1236, 1237, 1239 and 1241 ostracode Mg/Ca data, IGBP PAGES/World Data Center for Paleoclimatology, Data Contribution Series # 2009-011, NOAA/NCDC Paleoclimatology Program, Boulder CO, USA, 2009.
Dwyer, G. S. and Chandler, M. A.: Mid-Pliocene sea level and continental ice volume based on coupled benthic Mg/Ca palaeotemperatures and oxygen isotopes, Philos. T. R. Soc. A, 367, 157–168, 2009.
Emanuel, K.: Contribution of tropical cyclones to meridional heat transport by the oceans, J. Geophys. Res., 106(D14), 14771–14781, 2001.
Gradstein, F., Ogg, J., and Smith A.: A geologic time scale 2004, Cambridge, UK, Cambridge University Press, 589 p., 2004.
Haywood, A. M. and Valdes P. J.: Modelling Pliocene warmth: contribution of atmosphere, oceans and cryosphere, Earth Planet. Sc. Lett., 218, 363–377, 2004.
Hodell, D. A. and Ciesielski, P. F.: Stable isotopic and carbonate stratigraphy of the Plio-Pleistocene of the Ocean Drilling Program (ODP) Hole 704A: Eastern sub-Antarctic South Atlantic, Proceedings of the Ocean Drilling Program, Scientific Results, 114, 409–436,1991.
Jansen, E., Overpeck, J., Briffa, K. R., Duplessy, J. C., Joos, F., Masson-Delmotte, V., Olago, D., Otto-Bliesner, B., Peltier, W. R., Rahmstorf, S., Ramesh, R., Raynaud, D., Rind, D., Solomina, O., Villabla, R., and Zhang, D.: Palaeoclimate, in: Climate Change 2007: The Physical Science Basis. Contribution of Working Group I to the Fourth Assessment Report of the Intergovernmental Panel on Climate Change, edited by: Solomon, S., Qin, D., Manning, M., Chen, Z., Marquis, M., Averyt, K. B., Tignor, M., and Miller, H. L., Cambridge University Press, Cambridge, UK, 2007.





Karas, C., Nurnberg, D., Gupta, A. K., Tiedemann, R., Mohan, K., and Bickert, T.: Mid-Pliocene climate change amplified by a switch in Indonesian subsurface throughflow, Nat. Geosci., 2, 434–438, 2009.
Levitus, S. and Boyer, T. P.: World ocean atlas 1994 (4): temperature. NOAA Atlas NESDIS, 4, Washington, DC: US Department of Commerce, 1994.
Lisiecki, L. E. and Raymo, M. E.: A Pliocene-Pleistocene stack of 57 globally distributed benthic $d^{18}O$ records, Paleoceanography, 20, PA1003, doi:10.1029/2004PA001071, 2005.
Marotzke, J.: Abrupt climate change and thermohaline circulation: mechanisms and predictability, PNAS, 97, 1347–1350, 2000.
Martini, E.: Standard Tertiary and Quaternary calcareous nannoplankton zonation, in: Proc. II Int. Plankt. Conf., Roma, 1970, edited by: Ferinacci, A., Tecnoscienza, 2, 739–785, 1971.
Middleton, G. V.: Data analysis in the Earth Sciences using MATLAB. Prentice Hall, Upper Saddle River, New Jersey, 260 pp., 2000.
Oppo, D. W. and Fairbanks, R. G.: Variability in the deep and intermediate water circulation of the Atlantic Ocean during the past 25,000 years: Northern Hemisphere modulation of the Southern Ocean, Earth Planet. Sc. Lett. 86, 1–15, 1987.
Poore, H. R., Samworth, R. J., White, N. J., Jones, S. M. and McCave, I. N.: Neogene overflow of northern component water at the Greenland-Scotland ridge, Geochem. Geophys. Geosyst., 7, Q06010, doi:10.1029/2005GC001085, 2006.
Ridge, Geochem. Geophy. Geosy. 7, Q06010, doi:06010.01029/02005gc001085, 2006.
Ravelo, A. C., Dekens, P. S., and McCarthy, M.: Evidence for El Nino-like conditions during the Pliocene, GSA Today, 16, 4–11, 2006.
Raymo, M. E., Grant, B., Horrowitz, M., and Rau, G. H.: Mid-Pliocene warmth: stronger greenhouse and stronger conveyor, Mar. Micropaleontol., 27, 313–326, 1996.
Raymo, M. E., Ruddiman, W. F., Backman, J., Clement, B. M., and Martinson, D. G.: Late Pliocene variation in Northern Hemisphere ice sheets and North Atlantic deep water circulation, Paleoceanography, 4, 413–446, 1989.
Reynolds, R. W. and Smith, T. M.: A high-resolution global sea surface temperature climatology, J. Climate., 8, 1571–1583, 1995.
Robinson, M. M.: New quantitative evidence of extreme warmth in the Pliocene arctic, Stratigraphy, in press, 2009.
Robinson, M. M., Dowsett, H. J., and Chandler, M. A.: Pliocene role in assessing future climate impacts, EOS, 89, 501–502, 2008a.





Robinson, M. M., Dowsett, H. J., Dwyer, G. S., and Lawrence, K. T.: Reevaluation of mid-Pliocene North Atlantic sea surface temperatures, Paleoceanography, 23, PA3213, doi:10.1029/2008PA001608, 2008b.

Salzmann, U., Haywood, A. M., Lunt, D. J., Valdes, P. J., and Hill, D. J.: A new global biome reconstruction and data-model comparison for the Middle Pliocene, Global Ecol. Biogeogr., 17, 432–447, 2008.

Sancetta, C. and Silvestri, S.: High-resolution biostratigraphic and oceanographic events in the late Pliocene and Pleistocene North Pacific Ocean, Paleoceanography, 1, 163–180, 1986.

Sarnthein, M. and Fenner, J.: Global wind-induced change of deep-sea sediment budgets, new ocean production and $CO_2$ reservoirs ca. 3.3–2.35 Ma, Philo. T. R. Soc. B, 318, 487–504, 1988.

Shackleton, N. J., Hall, M. A., and Pate, D.: Pliocene stable isotope stratigraphy of Site 846, in, Pisias, N. G., Mayer, L. A., Janecsek, T. R., et al., Proceedings of the Ocean Drilling Program, Scientific Results, 138, 337–355, 1995.

Sohl, L. E., Chandler, M. A., Schmunk, R. B., Mankoff, K., Jonas, J. A., Foley, K. M., and Dowsett, H. J.: PRISM3/GISS topographic reconstruction, US Geol. Surv., Data Series 419, 6 pp., 2009.

Sriver, R. L. and Huber, M.: Observational evidence for an ocean heat pump induced by tropical cyclones, Nature, 447, 577–580, 2007.

Tiedemann, R., Sarnthein, M., and Shackleton, N.: Astronomical timescale for Pliocene Atlantic $d^{18}O$ and dust flux records of Ocean Drilling Program Site 659, Paleoceanography, 9, 619–638, 1994.

Toggweiler, J. R. and Russell, J.: Ocean circulation in a warming climate, Nature, 451, 286–288, 2008.

Wright, J. D. and Miller, K. G.: Control of North Atlantic Deep Water circulation by the Greenland-Scotland Ridge, Paleoceanography, 11, 157–170, 1996.





**Table 1.** PRISM3 SST estimates.

| | Locality | Latitude | Longitude | Water Depth (m) | Modern SST[1] Feb | Modern SST[1] Aug | Modern SST[2] Mean Annual | PRISM3 SST Feb[3] | PRISM3 SST MultiProxy[4] | PRISM3 SST Aug[3] | Selected Publications[5] |
|---|---|---|---|---|---|---|---|---|---|---|---|
| 1 | DSDP 310 | 36.87 | -176.90 | 3516.0 | 14.06 | 24.15 | 17.28 | 17.06 | - | 26.15 | [6] |
| 2 | ODP 886 | 44.69 | -168.24 | 5713.7 | 7.27 | 14.85 | 10.48 | 4.67 | - | 17.95 | [7] |
| 3 | DSDP 183 | 54.58 | -161.21 | 4708.0 | 2.88 | 11.31 | 7.48 | 1.68 | - | 13.61 | [7] |
| 4 | E14-8 | -59.67 | -160.29 | 3877.0 | 3.70 | 1.22 | 1.91 | >4.60 | - | - | [7] |
| 5 | Colvillian | 70.29 | -150.42 | 0.0 | -1.79 | -1.78 | 2.09 | 0.21 | - | 2.22 | [6] |
| 6 | ODP 887 | 54.37 | -148.45 | 3633.6 | 4.08 | 12.25 | 8.47 | 6.08 | - | 13.25 | [6] |
| 7 | DSDP 573 | 0.49 | -133.30 | 4301.0 | 25.62 | 24.90 | 25.90 | 24.62 | 24.70 | 24.70 | [8] |
| 8 | DSDP 36 | 40.98 | -130.12 | 3273.0 | 11.71 | 17.88 | 14.99 | 13.71 | - | 19.88 | [6] |
| 9 | ODP 1021 | 39.09 | -127.78 | 4213.0 | 11.64 | 16.99 | 14.50 | - | 21.50 | - | [8] |
| 10 | E13-17 | -65.68 | -124.11 | 4724.0 | 1.10 | -1.49 | -0.03 | <5.50 | - | - | [7] |
| 11 | ODP 1014 | 32.83 | -119.98 | 1165.7 | 14.32 | 18.27 | 16.10 | - | 24.00 | - | [8] |
| 12 | ODP 852 | 5.28 | -110.07 | 3860.1 | 27.09 | 26.74 | 27.00 | - | 29.40 | - | [8] |
| 13 | Meighen Island | 79.00 | -99.00 | 0.0 | -1.79 | -1.79 | -0.55 | 0.21 | - | 3.21 | [6] |
| 14 | DSDP 323 | -63.68 | -97.99 | 5004.0 | 3.19 | 0.44 | 1.85 | >4.39 | - | - | [6] |
| 15 | ODP 847 | 0.18 | -95.32 | 3334.5 | 26.06 | 22.10 | 24.40 | 28.45 | 26.90 | 25.72 | [8] |
| 16 | ODP 677 | 1.20 | -83.74 | 3472.5 | 26.27 | 25.58 | 25.60 | 28.91 | 27.50 | 26.67 | [8] |
| 17 | Sarasota | 27.25 | -82.66 | 0.0 | 20.48 | 29.36 | 25.36 | 19.88 | - | 26.96 | [6] |
| 18 | Pinecrest Beds | 27.35 | -82.43 | 0.0 | 20.48 | 29.36 | 24.36 | 20.48 | - | 29.36 | [6] |
| 19 | Cayo Aqua | 9.15 | -82.05 | 0.0 | 27.99 | 28.38 | 27.59 | 27.99 | - | 29.50 | [6] |
| 20 | SEFlor(G-182) | 25.78 | -80.28 | 0.0 | 23.34 | 29.57 | 26.25 | 21.34 | - | 30.00 | [6] |
| 21 | DSDP 502 | 11.49 | -79.38 | 3051.0 | 26.65 | 28.10 | 27.69 | 27.80 | - | 27.57 | [9] |
| 22 | Duplin | 34.00 | -79.00 | 0.0 | 20.41 | 28.57 | 23.54 | 19.71 | - | 28.17 | [6] |
| 23 | Lee Creek | 35.38 | -76.75 | 0.0 | 14.46 | 27.03 | 21.10 | 16.76 | - | 30.13 | [6] |
| 24 | Yorktown | 37.00 | -76.50 | 0.0 | 10.11 | 25.93 | 19.89 | 15.31 | - | 27.73 | [6] |
| 25 | ODP 1237 | -16.00 | -76.37 | 3212.3 | 23.06 | 16.39 | 20.00 | 28.37 | 23.20 | 21.90 | [8] |
| 26 | DSDP 603 | 35.49 | -70.03 | 4633.0 | 19.94 | 27.08 | 22.57 | 25.24 | 23.70 | 27.53 | [9] |
| 27 | DSDP 541 | 15.52 | -58.72 | 4940.0 | 25.97 | 28.11 | 27.11 | 27.84 | 21.73 | 27.56 | [9] |
| 28 | ODP 672 | 15.50 | -58.50 | 4982.5 | 25.97 | 28.11 | 27.11 | 27.57 | 21.73 | 26.88 | [9] |
| 29 | ODP 646 | 58.25 | -48.33 | 3440.3 | 2.15 | 7.37 | 5.41 | 3.62 | - | 9.54 | [6] |
| 30 | DSDP 396 | 22.90 | -43.50 | 4459.0 | 23.46 | 26.39 | 24.88 | 24.75 | - | 27.53 | [6] |
| 31 | ODP 695 | -62.39 | -43.45 | 1300.1 | 0.05 | -1.79 | 0.00 | <4.72 | - | - | [6] |
| 32 | DSDP 606 | 37.34 | -35.50 | 3007.0 | 16.50 | 24.37 | 20.50 | 18.30 | 21.90 | 25.50 | [10] |
| 33 | DSDP 516 | -30.27 | -35.28 | 1313.0 | 23.98 | 18.48 | 22.25 | 26.00 | - | 20.50 | [6] |
| 34 | DSDP 607 | 41.00 | -32.96 | 3427.0 | 15.34 | 22.86 | 18.80 | 16.20 | 19.80 | 23.30 | [10] |
| 35 | ODP 699 | -51.54 | -30.68 | 3705.5 | 3.83 | 1.00 | 3.63 | 5.80 | - | - | [7] |
| 36 | DSDP 410 | 45.51 | -29.48 | 2976.0 | 13.34 | 19.21 | 15.86 | 16.10 | - | 25.00 | [6] |
| 37 | DSDP 609 | 49.88 | -24.24 | 3883.5 | 11.48 | 16.55 | 14.10 | 14.60 | 18.70 | 22.80 | [10] |
| 38 | DSDP 552 | 56.04 | -23.23 | 2301.0 | 9.07 | 13.33 | 11.60 | 12.80 | 16.70 | 21.00 | [10] |
| 39 | DSDP 608 | 42.84 | -23.09 | 3526.0 | 13.68 | 20.70 | 17.11 | 17.76 | - | 25.60 | [7] |
| 40 | ODP 667 | 4.55 | -21.90 | 3524.9 | 27.34 | 26.81 | 27.50 | 27.28 | - | 26.79 | [9] |
| 41 | ODP 659 | 18.08 | -21.03 | 3071.7 | 20.94 | 24.47 | 22.42 | 22.26 | - | 27.66 | [9] |
| 42 | DSDP 366 | 5.68 | -19.85 | 2853.0 | 27.32 | 26.81 | 27.47 | 27.84 | - | 27.20 | [7] |
| 43 | ODP 661 | 9.45 | -19.39 | 4012.9 | 24.81 | 26.91 | 26.49 | 27.12 | - | 26.72 | [9] |
| 44 | DSDP 610 | 53.22 | -18.89 | 2426.3 | 10.49 | 14.98 | 13.15 | 14.16 | - | 24.33 | [9] |
| 45 | Tjornes | 66.16 | -17.25 | 0.0 | 1.35 | 7.38 | 4.39 | 5.35 | - | 13.58 | [6] |
| 46 | ODP 693 | -70.83 | -14.57 | 2359.0 | -0.92 | -1.79 | -0.48 | <4.28 | - | - | [7] |
| 47 | DSDP 548 | 48.85 | -12.00 | 1251.0 | 11.34 | 17.18 | 14.14 | 18.31 | - | 27.62 | [9] |
| 48 | DSDP 521 | -26.07 | -10.27 | 4127.5 | 24.74 | 19.45 | 22.89 | 26.74 | - | 21.45 | [6] |
| 49 | DSDP 546 | 33.80 | -9.60 | 3958.0 | 16.73 | 22.33 | 18.95 | 19.11 | - | 24.17 | [9] |
| 50 | ODP 690 | -65.16 | 1.21 | 2914.0 | 0.90 | -1.79 | 0.00 | <5.80 | - | - | [7] |
| 51 | North Sea | 52.50 | 1.50 | 0.0 | 5.71 | 16.34 | 10.97 | 10.41 | - | 16.74 | [6] |
| 52 | ODP 909 | 78.58 | 3.07 | 2518.6 | -1.80 | -0.74 | 0.79 | - | 13.20 | - | [11] |
| 53 | ODP 704 | -46.88 | 7.42 | 2532.3 | 7.07 | 4.81 | 6.72 | 9.57 | - | 7.31 | [6] |
| 54 | PS1448 | -58.64 | 7.92 | 4970.0 | 1.06 | -1.75 | -0.18 | <4.03 | - | - | [6] |
| 55 | ODP 911 | 80.47 | 8.23 | 901.5 | -1.79 | -1.67 | -0.03 | - | 18.10 | - | [11] |
| 56 | DSDP 532 | -19.74 | 10.52 | 1331.0 | 20.88 | 15.79 | 18.82 | 22.68 | - | 17.59 | [6] |
| 57 | DSDP 132 | 40.25 | 11.43 | 2835.0 | 13.78 | 25.04 | 18.74 | 15.38 | - | 26.64 | [7] |
| 58 | ODP 907 | 69.25 | 12.70 | 1801.2 | 5.85 | 10.91 | 3.23 | - | 11.70 | - | [11] |
| 59 | Punta di Maiata | 37.33 | 13.50 | 0.0 | 14.62 | 25.75 | 19.61 | 17.50 | - | 21.27 | [7] |
| 60 | Punta Piccola | 37.33 | 13.58 | 0.0 | 14.62 | 25.75 | 19.61 | 18.84 | - | 23.88 | [7] |
| 61 | Finikia | 35.25 | 25.17 | 0.0 | 15.41 | 24.31 | 20.43 | 16.14 | - | 19.90 | [7] |
| 62 | ODP 722 | 16.62 | 59.80 | 2022.1 | 25.00 | 24.77 | 26.84 | 26.05 | - | 27.04 | [7] |
| 63 | ODP 736 | -49.40 | 71.66 | 628.7 | 4.48 | 1.77 | 3.74 | <7.48 | - | - | [6] |
| 64 | ODP 747 | -54.81 | 76.79 | 1695.8 | 2.41 | 0.14 | 1.90 | >4.51 | - | - | [6] |
| 65 | ODP 748 | -58.44 | 78.98 | 1289.6 | 1.44 | -1.70 | 1.15 | <4.64 | - | - | [6] |
| 66 | ODP 751 | -57.73 | 79.81 | 1633.8 | 1.69 | -1.33 | 1.21 | <4.59 | - | - | [6] |
| 67 | ODP 745 | -59.60 | 85.86 | 4082.5 | 1.84 | -1.55 | 1.06 | <4.74 | - | - | [6] |
| 68 | DSDP 266 | -56.40 | 110.11 | 4167.0 | 3.48 | 0.66 | 1.82 | >4.68 | - | - | [6] |
| 69 | ODP 769 | 8.78 | 121.29 | 3644.0 | 26.89 | 28.73 | 28.70 | 26.89 | 28.10 | 29.23 | [8] |
| 70 | DSDP 445 | 25.52 | 133.20 | 3377.0 | 20.98 | 28.46 | 25.60 | 22.98 | 26.30 | 29.46 | [8] |
| 71 | Yabuta | 37.00 | 137.00 | 0.0 | 9.86 | 24.95 | 17.81 | 9.86 | - | 24.95 | [6] |
| 72 | Sasaoka | 39.50 | 140.50 | 0.0 | 7.01 | 22.12 | 16.62 | 8.51 | - | 24.12 | [6] |
| 73 | E50-28 | -62.90 | 150.68 | 3489.0 | 1.87 | -1.69 | 0.98 | <4.97 | - | - | [6] |
| 74 | E36-33 | -57.75 | 150.88 | 3952.0 | 3.67 | 0.84 | 3.21 | >4.67 | - | - | [7] |
| 75 | DSDP 579 | 38.63 | 153.84 | 5737.0 | 12.03 | 23.33 | 17.27 | 17.53 | - | 27.73 | [6] |
| 76 | DSDP 580 | 41.63 | 153.98 | 5375.0 | 6.19 | 19.79 | 13.43 | 12.39 | - | 23.09 | [6] |
| 77 | DSDP 586 | -0.50 | 158.50 | 2207.0 | 29.26 | 29.01 | 29.20 | 29.26 | 29.20 | 29.01 | [8] |
| 78 | ODP 806 | 0.31 | 159.36 | 2520.5 | 29.16 | 29.00 | 29.20 | 28.96 | 29.60 | 28.32 | [8] |
| 79 | ODP 881 | 47.10 | 161.49 | 5530.9 | 2.44 | 12.11 | 6.78 | 4.34 | - | 15.91 | [6] |
| 80 | E. Kamchatka | 56.00 | 163.00 | 0.0 | 0.11 | 11.35 | 7.45 | 4.11 | - | 10.85 | [6] |
| 81 | Karaginsky | 58.85 | 164.04 | 0.0 | -0.94 | 11.26 | 6.41 | 3.06 | - | 13.26 | [6] |
| 82 | DSDP 592 | -36.47 | 165.44 | 1088.0 | 20.33 | 15.11 | 18.28 | 22.33 | - | 17.11 | [7] |
| 83 | ODP 883 | 51.20 | 167.77 | 2390.8 | 2.71 | 10.38 | 6.45 | 3.20 | - | 14.90 | [6] |
| 84 | E50-33 | -61.09 | 170.06 | 4550.0 | 4.00 | 0.24 | 3.02 | >4.50 | - | - | [7] |
| 85 | DSDP 274 | -68.99 | 173.43 | 3305.0 | -0.48 | -1.79 | -0.40 | <4.52 | - | - | [7] |
| 86 | Rangitikei R. | -39.50 | 175.87 | 0.0 | 17.97 | 13.23 | 16.12 | 19.97 | - | 15.23 | [7] |





**Table 2.** Deep Ocean Temperature estimates.

| | Locality | Latitude | Longitude | Water Depth (m) | Maximum 10%[1] Anomaly | Maximum 10%[1] Temperature | Water[2] Mass | Selected Publications[3] |
|---|---|---|---|---|---|---|---|---|
| 1 | IODP 1123 | -41.79 | -171.50 | 3290.1 | 1.2 | 2.7 | CPDW | [4] |
| 2 | IODP 1241 | 5.84 | -86.44 | 2027.3 | 0.2 | 2.5 | PCW | [4] |
| 3 | IODP 1239 | -0.67 | -82.08 | 1414.7 | 0.3 | 3.6 | PCW | [4] |
| 4 | IODP 1236 | -21.36 | -81.44 | 1323.7 | -1.9 | 1.4 | AAIW/PCW | [4] |
| 5 | DSDP 502 | 11.49 | -79.38 | 3051.0 | -0.9 | 3.2 | AIW | [5] |
| 6 | IODP 1237 | -16.01 | -76.38 | 3212.7 | 0.9 | 2.5 | PCW/CPDW | [4] |
| 7 | ODP 928 | 5.46 | -43.75 | 4011.0 | 1.2 | 3.4 | NADW | [4] |
| 8 | ODP 929 | 5.98 | -43.74 | 4356.0 | 0.3 | 2.5 | NADW/AABW | [4] |
| 9 | ODP 925 | 4.20 | -43.49 | 3041.0 | 2.0 | 4.7 | NADW | [6] |
| 10 | ODP 926 | 3.72 | -42.91 | 3598.0 | 2.0 | 4.5 | NADW | [6] |
| 11 | DSDP 607 | 41.00 | -32.96 | 3427.0 | 1.5 | 4.0 | NADW | [5, 6] |
| 12 | DSDP 552 | 56.04 | -23.23 | 2301.0 | 3.2 | 6.3 | UNADW | [5] |
| 13 | ODP 659 | 18.08 | -21.03 | 3072.0 | -0.5 | 2.3 | NADW | [5] |
| 14 | ODP 661 | 9.45 | -19.39 | 4013.0 | 0.3 | 2.7 | NADW | [5] |
| 15 | DSDP 610 | 53.22 | -18.89 | 2417.0 | 0.2 | 3.3 | NADW | [5] |
| 16 | ODP 658 | 20.75 | -18.58 | 2263.0 | 1.7 | 4.9 | NADW | [5] |
| 17 | ODP 982 | 57.52 | -15.87 | 1134.0 | -1.0 | 4.6 | UNADW | [4] |
| 18 | ODP 959 | 3.63 | -2.74 | 2091.0 | 0.6 | 4.1 | AAIW/NADW | [4] |
| 19 | IODP 1092 | -46.41 | 7.08 | 1973.0 | -0.6 | 1.7 | CPDW/NADW | [4] |
| 20 | ODP 704 | -46.88 | 7.42 | 2532.0 | 4.2 | 6.1 | NADW | [5] |
| 21 | IODP1090 | -42.91 | 9.00 | 3700.0 | 0.4 | 2.0 | NADW/CPDW | [4] |
| 22 | IODP 1085 | -29.37 | 13.99 | 1713.0 | 0.3 | 3.3 | CPDW | [4] |
| 23 | ODP 754 | -30.94 | 93.57 | 1063.6 | -0.3 | 4.8 | SURF/AAIW | [4] |
| 24 | ODP 806 | 0.32 | 159.36 | 2520.7 | 0.9 | 2.8 | PDW | [4] |
| 25 | ODP 805 | 1.23 | 160.53 | 3188.5 | 0.5 | 2.3 | PDW | [4] |
| 26 | ODP 804 | 0.94 | 161.65 | 3861.7 | 0.3 | 1.9 | PDW | [4] |
| 27 | DSDP 592 | -36.47 | 165.44 | 1088.0 | -2.1 | 3.3 | SURF/AAIW | [4] |





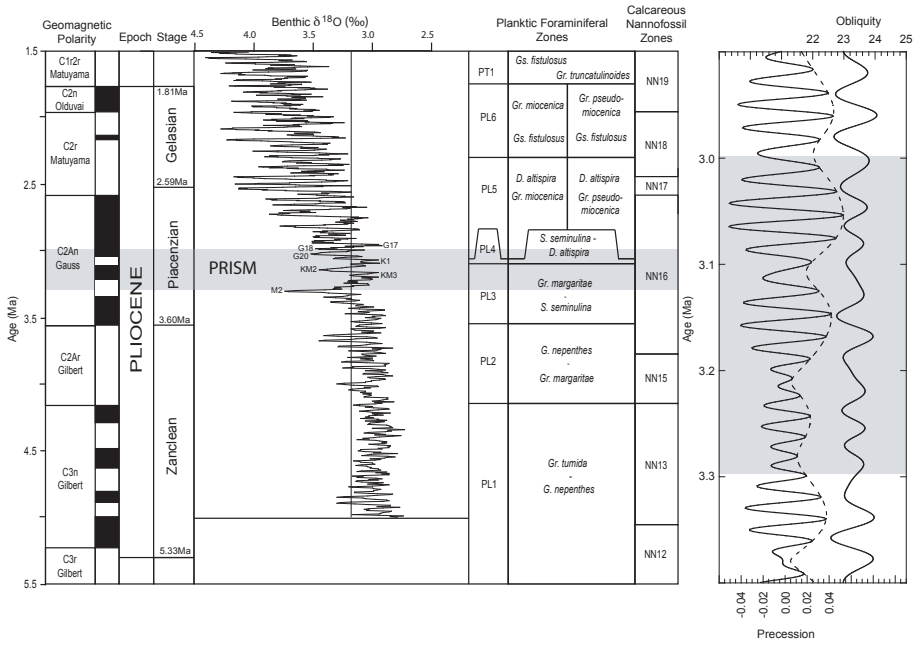


**Fig. 1.** Pliocene magnetobiostratigraphic framework after Berggren et al. (1995). Gray band approximates the PRISM time slab. Benthic d$^{18}$O record from Lisiecki and Raymo (2005). Position of PRISM time slab (shaded horizontal band) relative to geomagnetic polarity, planktic foraminiferal zones, calcareous nannofossil zones and orbital geometry (Berggren, 1973, 1977; Berggren et al., 1995; Martini, 1971). Note low-amplitude obliquity cycles throughout the mid-Piacenzian with precessional cycles that build in amplitude from the earlier to later part of the PRISM time slab. Eccentricity is shown by dashed line tracing upper limit of precession (Dowsett et al., 2005). Figure modified from Dowsett et al. (2005) and Dowsett and Robinson (2006).



CPD
5, 1901–1928, 2009

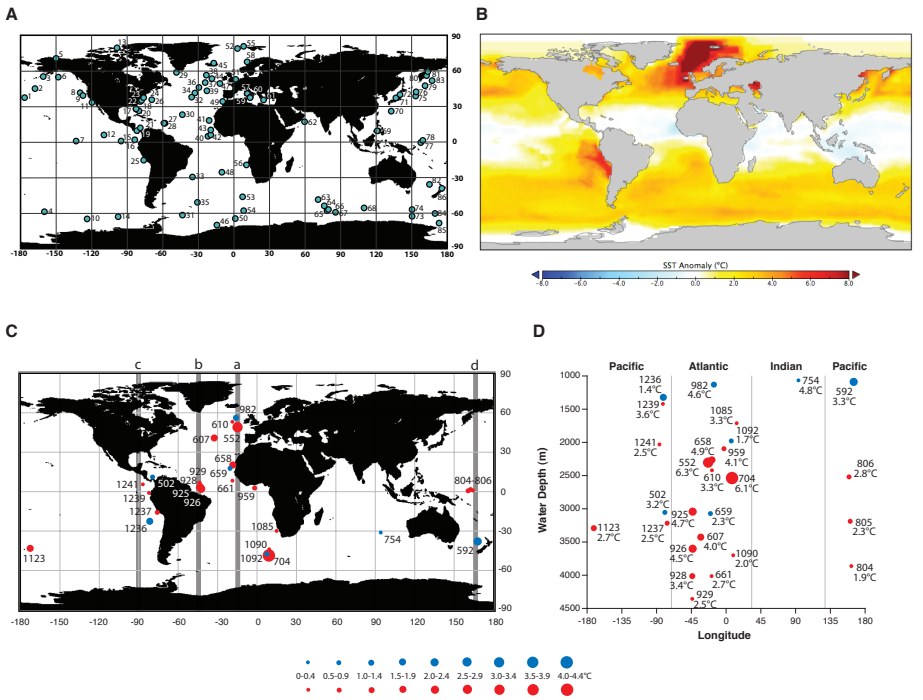


**Fig. 2.** **(A)** Location of sites used for surface temperature reconstruction. **(B)** Pliocene estimated 1 December surface temperature anomaly based upon PRISM3 SST reconstruction. **(C)** Location of sites utilized in deep ocean temperature analysis. Size of dots indicate magnitude of temperature anomaly (Pliocene minus present day); blue=cooler than modern, red=warmer than modern. Lines a–d show position of longitudinal transects given in Fig. 3. **(D)** Maximum (top 10%) mid-Piacenzian deep ocean temperature estimates by water depth from all sites, projected onto an equatorial plane. Symbols are in **(C)**.



CPD
5, 1901–1928, 2009

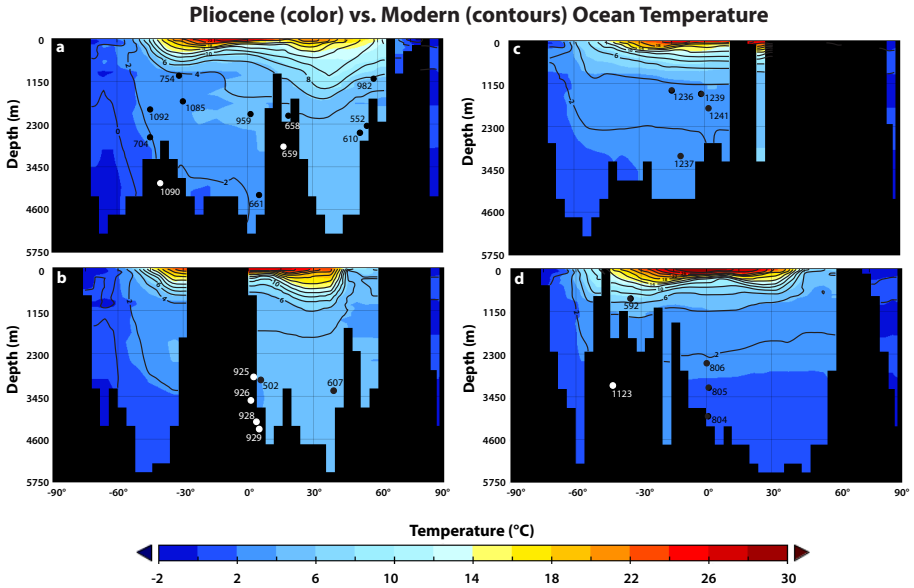


**Fig. 3.** Longitudinal profiles of ocean temperature from transects shown in Fig. 2c: **(a)** 15° W, **(b)** 45° W, **(c)** 90° W and **(d)** 165° E. All temperatures are shown in °C. Contour interval is 2°C. Black contour lines show modern temperature overlaid on colored regions showing the mid-Piacenzian reconstruction. The change in temperature can be surmised by comparing the color contours to the black overlaid contour lines. For example, in panel d, Site 806 is slightly cooler than 2°C in the modern ocean but was slightly warmer than 2°C during the mid-Piacenzian. Actual estimates at all sites are shown in Fig. 2d and given in Table 2.



CPD
5, 1901–1928, 2009